

Crystal Growth in the Foliated Aragonite of Monoplacophorans (Mollusca)

Antonio G. Checa,^{*,†} Antonio Sánchez-Navas,[‡] and Alejandro Rodríguez-Navarro[‡]

[†]Departamento de Estratigrafía y Paleontología and [‡]Departamento de Mineralogía y Petrología, Facultad de Ciencias, Universidad de Granada, Avenida Fuentenueva s/n, 18071 Granada, Spain

Received June 2, 2009; Revised Manuscript Received September 4, 2009

ABSTRACT: Crystal-growth features of the foliated aragonite from two species of the rare monoplacophoran molluscs have been analyzed. The crystals have unique morphologies. They are very thin along the *c* axis and elongated along the *a* axis, and their arrangement varies depending on the species. Surface energy minimization in the crystal arrangement observed in *Micropilina* leads to a discrete number of constant angular relationships, which is explained by twin laws and epitaxy. Textural analysis shows that crystals form oriented aggregates with their *c* axes perpendicular to the shell surface. Close to the shell margin, crystals compete so as to orient their *a* axes nearly perpendicular to the growth front of the lamellae, although the scattering of the *a* axis soon increases toward the shell interior. In contrast to inorganic crystals, growth along the *c* axis is inhibited by organic molecules. Their incorporation may be related to the existence of weak intermolecular interactions between CO₃ groups along this axis. Conversely, there is no chemical affinity to incorporate organic molecules along the *a* axis, where particularly short CO₃–Ca ionic bonds occur. These structural factors explain the formation of crystals which are elongated and free of organic inclusions along the *a* axis.

1. Introduction

Mollusk shells are highly sophisticated composite materials formed by CaCO₃ crystals embedded within an organic framework. Shells are made of superimposed layers having a monomineral composition (either calcite or aragonite) and formed by crystals of uniform size and morphology which are arranged in an ordered manner according to different architectures or shell microstructures.^{1a,b} Particular shell microstructures are characteristic of calcitic (i.e., prismatic, foliated) and aragonitic (i.e., nacre, crossed-lamellar) layers. In these biomaterials, the mineral and the organic matrix are intimately associated and hierarchically organized from the nano- to the millimeter scale.^{2a,b} For a given mollusc species, shell microstructural characteristics are precisely defined and constant, indicating that the animal controls the process of mineralization in an exhaustive way.³

Shell mineralization occurs within a closed environment delimited by the mantle, in which a solution of complex composition is secreted by this tissue. This solution is the extrapallial fluid and contains calcium and carbonate ions for the precipitation of calcium carbonate crystals, as well as the organic precursors necessary for the formation of the organic matrix. There is evidence from in vitro CaCO₃ crystallization tests that specific proteins of the organic matrix play a mayor role in the control of shell mineralization and specifically regulate crystal growth by defining the polymorphic phase, size, and morphology of calcium carbonate crystals that make up the mollusc shell layers.^{4a–c} On the other hand, the ordered assembly of the crystals suggests that complex processes are accorded in space and time, resulting in a material with well-defined microstructural characteristics.^{5a,b} However, an understanding of the exact mechanisms by which molluscs control crystal growth and at the same time direct the ordered assemblage of crystals and the organic matrix according to a particular microstructure type is still lacking.

Some shell microstructures are better characterized than others. For instance, regarding aragonitic microstructures, nacre is the most intensively scrutinized microstructure and is well characterized in a number of studies describing its organization and growth mechanisms.^{2b,4c,6a,b} However, other common aragonitic microstructures have been poorly studied. This is the case of the foliated aragonite, the material examined in this study. It is secreted exclusively by present-day monoplacophorans, a group of so-called living fossils, the first representative of which was dredged in 1952 from deep waters off the coast of Costa Rica. Since then, some 20 living species grouped in seven genera have been described. They are today considered to comprise a separate Order (Tryblidiida), within the molluscan Class Tergomya,⁷ dating back to the Middle Cambrian.

Monoplacophorans have small cap-shaped shells, with the apex pointing in the anterior direction (Figure 1). According

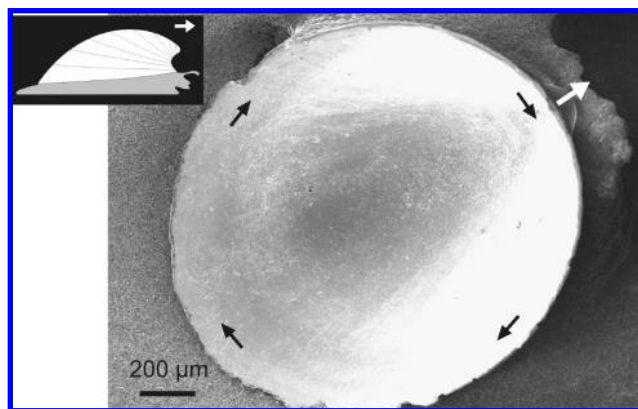


Figure 1. General view of the internal surface of the shell of *Rokopella euglypta*. Black arrows indicate local growth directions of the lamellae, which are perpendicular to the radial growth direction of the shell. The small sketch shows the orientation of the animal in its shell during life. The white arrows indicate the anterior direction.

*To whom correspondence should be addressed. E-mail: aheca@ugr.es; tel.: +34 958243201; fax: +34 958 248528.

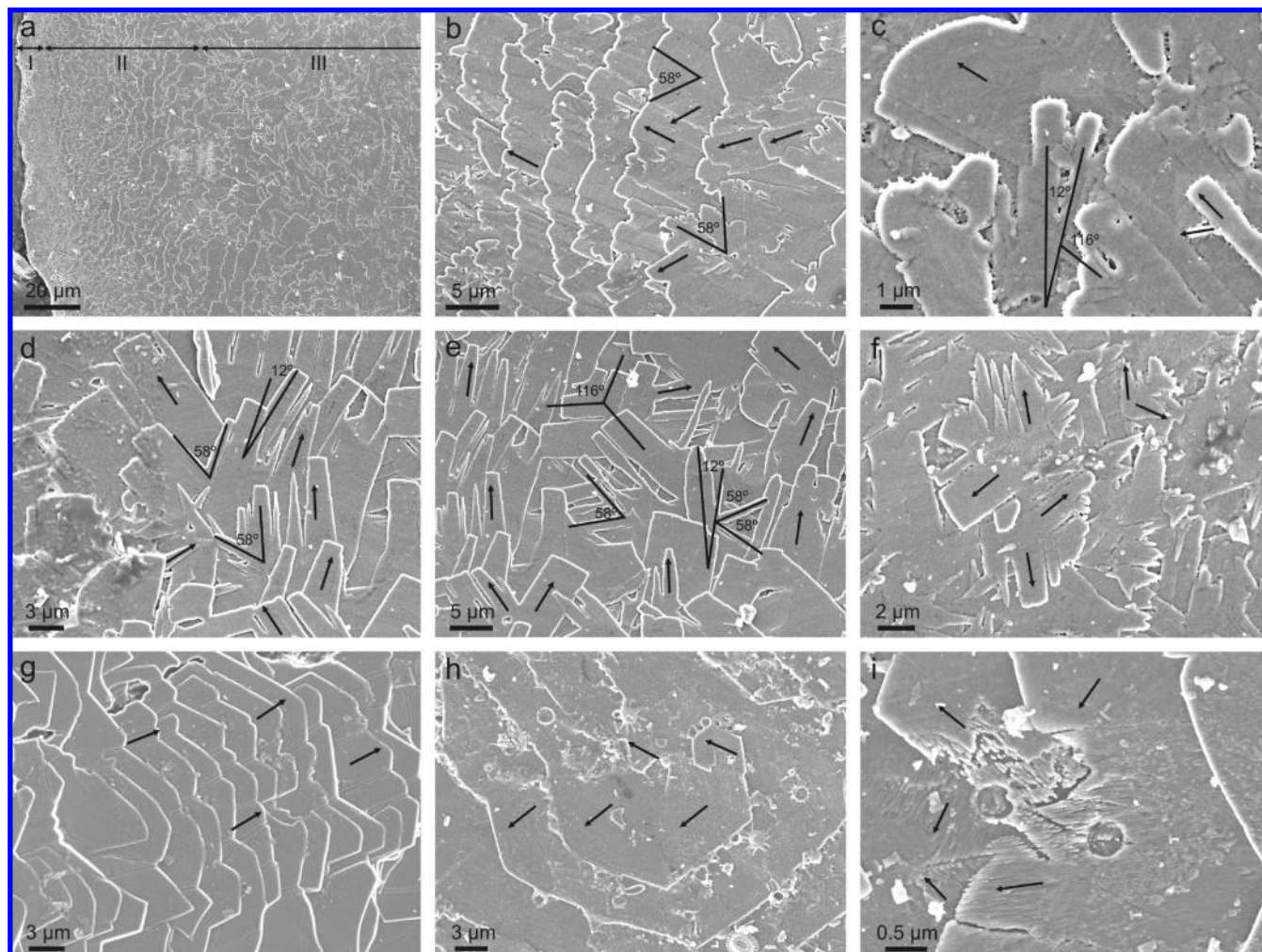


Figure 2. Secondary electron images of the shell interiors of *Micropilina arntzi* (a–f) and *Rokopella euglypta* (g–i). (a) Marginal posterior area, with indication of (I) external shell layer, (II) outer and (III) inner areas of the internal aragonitic foliated layer. (b) Detail of area II, with laths preferentially oriented parallel to the local direction of shell growth. Frequent angular relations at about 58° are observed between lath-like crystals, with the $\{010\}$ face of one crystal leaning against the $\{110\}$ face of its neighbor. (c–f) Views of area III, showing a complex intertwined arrangement of crystals, despite which persistent angular relationships between laths at 12° , 58° , and 116° (indicated in some instances) are observed. (g–i) Crystals with well-developed $\{110\}$ faces are observed in *Rokopella euglypta*. (g) Laths are strictly oriented along the a axis in the marginal posterior area, where crystals share their $\{010\}$ faces. (h) Pile of pseudo-hexagonal plates in the inner shell areas. (i) Detail of naturally etched plates [same area as in (h)] showing lineations parallel to the a axis. Arrows indicate the orientation of lineations of some selected examples. Constant angular relationships at 60° and 120° are observed.

to previous knowledge, the shells of monoplacophorans had an internal nacreous layer.^{8a–f} Thus, it seemed that the group retained the condition considered to be ancestral in molluscs. Checa et al.⁹ realized that what was usually described as monoplacophoran nacre is in fact a different kind of material, which these authors named foliated aragonite. Contrary to the typical nacre tablets, foliated aragonite is formed by flat laths (Figure 2). As in nacre tablets, foliated laths are very short along the 001 direction ($0.25\text{--}0.35\ \mu\text{m}$), but elongated widely in parallel to the a axis. These laths arrange in layers and the degree of misorientation of the crystals varies according to their position on the shell.

The study of the foliated aragonite of monoplacophorans is important in two main respects. First, monoplacophorans are considered as a basal clade of molluscs, making foliated aragonite an ancient biomaterial within the group. Its affinities and relationships to other molluscan biomaterials, such as nacre, thus constitute central themes in evolutionary studies. Second, from the standpoint of biomineralization,

the study of novel and/or poorly characterized biomaterials, such as foliated aragonite, deserves particular attention. It is particularly relevant from the crystallographic viewpoint, given the varied and intricate crystal morphologies and orientations found in foliated aragonite.⁹

This paper focuses mainly on investigating the factors controlling the development of the foliated aragonite in two monoplacophoran species. Because of its singular crystallographic features, foliated aragonite of monoplacophorans is unique in nature. In particular, the blade-like morphology of the aragonite crystals forming this microstructure has not been observed in any other aragonite-based material. Thus, there is a need to identify the crystal-growth mechanisms and processes responsible for these morphological features and for the ordered assemblage of crystals in this peculiar configuration. In particular, to understand the mechanisms for the organization of this material, we have studied it at different stages of development using field emission scanning electron microscopy (FE-SEM) and electron backscatter

diffraction (EBSD) techniques, which provide detailed information concerning the microstructure and crystallographic relations in this material. Additionally, we gain insight from the comparison of the different crystal morphologies observed in the two monoplacophoran species studied. Such a study may provide useful information for the understanding of the kinetics and structural control of crystal growth in biomaterials.

2. Material and Methods

2.1. Material. We have examined three empty shells of *Rokopella euglypta* coming from the Atlantis Bank, NO of “le Suroli”, Seamount 2, DW 261 (coordinates 34°22.40'N, 30°27'80"W), from a depth of 1340 m. They were collected by Serge Gofas, Bernard Métiévier, and Anders Warén (1993-02-03) and deposited in the Muséum National d'Histoire Naturelle Paris. In addition, two specimens of *Micropilina arntzi* were studied. They come from Antarctica, Lazarev Sea (coordinates 69°57.5' S, 6°20.0' E), from a depth of 280–298 m. They were collected by Stefan Hain, (1991-02-23) during the expedition R/V Polarstern ANT IX/3 1991, and are presently deposited in the Swedish Museum of Natural History (SMNH), under type No. 4858.

2.2. Scanning Electron Microscopy. Scanning electron microscopy (SEM) was used both for fractured specimens and for the shells' interiors. Samples were usually observed intact, although in some we removed the organic matter (with 5% NaOCl from 5 to 15 min). Samples were coated with carbon (Hitachi UHS evaporator) for variable pressure SEM (VPSEM) (Leo 1430-VP) or FE-SEM observation (Leo Gemini 1530).

2.3. Electron Diffraction. EBSD analyses the diffraction pattern produced when backscattered electrons are diffracted by a crystalline material. This pattern, once indexed, provides information on the orientation of the crystal lattice. Data from different positions can either be integrated into an orientation map or be processed to represent pole figures in stereographic projection. Samples were analyzed unpolished and only the organic matter was removed from the samples prior to analysis. The equipment used is an Inca Crystal (Oxford Instruments) detector coupled to a Gemini-1530 (Carl Zeiss) FESEM (CSIRC, Universidad de Granada).

3. Results

3.1. SEM Results. *Micropilina arntzi*. Units composing the foliated aragonite are very elongated, flat ($\sim 0.4 \mu\text{m}$ thick) laths, which are much longer than wide (Figure 2a,b). The mean width of laths is 3–4 μm , although extreme values range from $< 0.5 \mu\text{m}$ to $> 25 \mu\text{m}$ (Figure 2a–f). Their contour is typically rectangular, with straight to slightly arcuate growth fronts (Figure 2a–f). In some instances the lath is pointed, due to convergence of the sides toward the growth front (Figure 2d,f). The arrangement of laths is variable from the shell edge to the interior. Close to the contact with the outer shell layer, laths are coplanar and arranged into lamellae with comarginal growth fronts, which have a step-like distribution. The general orientation of the elongation axis of laths is perpendicular to the growth fronts of lamellae, although it is not infrequent for crystals directions to diverge at an angle close to 60° (Figure 2b). This arrangement, found in a marginal position (ca. 50 μm wide), has been labeled as I in Figure 2a. More to the shell interior (band II in Figure 2a), the arrangement is much more complex. The distribution into lamellae becomes obscure because laths usually divide or juxtapose or even intercept each other (Figure 2d–f). Very frequently, a lath constitutes the central member that branches at some 60° , on one or on both sides, forming an intertwined array (Figure 2e,f). In some such instances, in which the contacts between crystals are visible, it is clear that the side laths in fact juxtapose to the central lath (Figure 2b,c). In rare instances, crystals meet or divide at lesser angles ($\sim 10^\circ$) (Figure 2b).

***Rokopella euglypta*.** Toward the shell edges, crystals are elongated, flat ($\sim 0.25 \mu\text{m}$ thick) laths (Figure 2g). Crystals may reach lengths $> 100 \mu\text{m}$, while their width varies between < 1 and 12 μm (Figure 2g). The growth fronts of individual laths change from arcuate to arrowhead (Figure 2g). The crystals are coplanar and arranged into

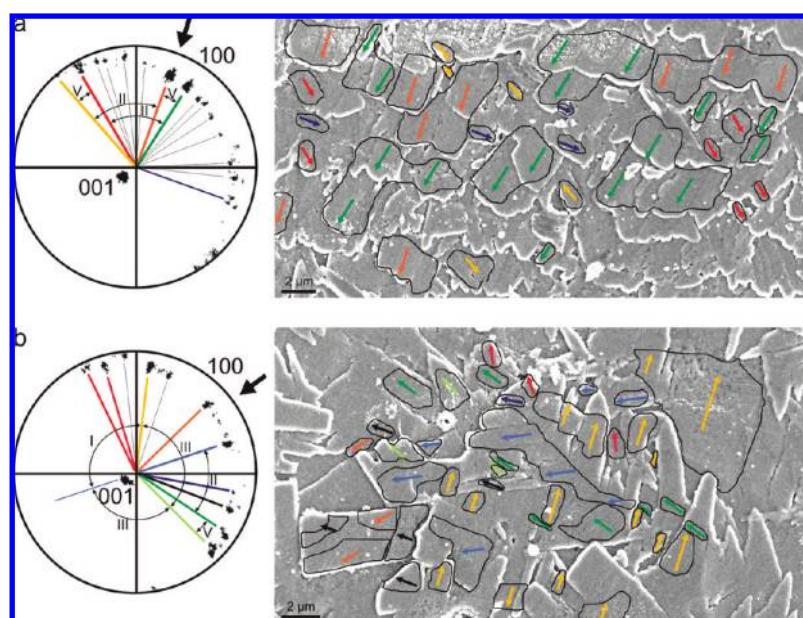


Figure 3. EBSD data on *Micropilina arntzi*. Left, 100 and 001 pole figures, with indications of the diverse types of angular relations between the most important maxima; thick arrows indicate the local growth directions of the shell. Right, secondary electron images of the areas mapped; each crystal has been assigned the exact orientation of its *a* axis according to the EBSD orientation map. Arrowheads indicate the growth direction of crystals. The correspondence between crystals and 100 maxima can be discerned after the color arrows and lines. (a) Marginal area of the foliated aragonitic layers (area II in Figure 2a). (b) Internal shell area (area III in Figure 2a). The pole figures also show the *c* axes of aragonite in a circa-zenithal position.

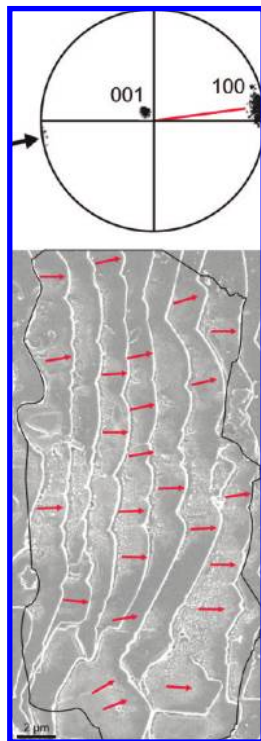


Figure 4. EBSD data on the marginal area of *Rokopella euglypta*. Top, 100 and 001 pole figure; there is a single broad 100 maximum. Bottom, secondary electron image of the area mapped; each crystal has been assigned the exact orientation of its *a* axis (arrows) according to the EBSD orientation map. Arrowheads indicate the growth direction of crystals. The pole figures show that the *a* axes are parallel to the growth direction of lamellae (thick arrow) and that the *c* axes are in a circa-zenithal position.

lamellae. All crystals are evenly oriented and, contrary to *Micropilina*, are able to expand laterally, so as to fill all of the available lamellar surface. All around the shell, the crystals grow parallel to the margin, in a sort of circumferential (clockwise) growth (Figure 1). Closer to the shell center, the stepped lamellae are progressively replaced by large flat plates with diameters of tens of micrometers, which occasionally display spiral growth (Figure 2h). When such plates are naturally corroded, a nanostructure in the form of nanometric needles is visible (Figure 2i). The angle of divergence of the needles (parallel to the *a* axis; unpublished results) in adjacent crystals is commonly found to be about 60° or 120°.

3.2. EBSD Results. In *Micropilina arntzi* the different orientation maps display similar results. Single crystals display coherent orientations and elongate along the *a* axis. Two large-sized maps, one close to the shell margin (i.e., within band II in Figure 2a) (Figure 3a), and the other at an intermediate position toward the shell interior (band III in Figure 2a) (Figure 3b) provide similar results (Figure 3). The 001 maxima are close to the centers of the pole figures, thus implying that the *c* axis is nearly perpendicular to the main surfaces of the laths. The maxima displayed in the 100 pole figures are ring-like, although, notably, they are not dispersed, but grouped into discrete maxima at every 5 to 10 degrees, despite the high number of crystals mapped. The main difference between the two maps measured in the different locations relates to the sizes of maxima. In the map made in the marginal area of the shell (Figure 3a), there are two nearby big maxima at ~12°, which group most data.

They roughly coincide with the overall growth direction of the lamellae (large arrow in Figure 3a). The superposition of the orientations of *a* axes onto the SEM image (Figure 3a, right) provides a qualitative view of the abundance of crystals oriented in the different directions and of the relationships between crystal groups. The map made closer to the central area (Figure 3b) also shows a circular distribution of the discrete maxima, but it is not possible to establish differences relative either to the importance of the recorded maxima or to the relationship among crystal groups with any particular common orientation. The superposition of the *a* axes onto the mapped crystals (Figure 3b, right) gives an idea of the absence of dominant orientations.

Orientation maps close to the edge of the shell of *Rokopella euglypta* (Figure 4) show that, as in *Micropilina*, single tablets are coherently oriented and that they have their *a* axes invariably parallel to their main elongations.⁹ The corresponding 001 and 100 pole figures display discrete maxima (Figure 4, top), indicating that the *c* axis is almost perpendicular to the shell surface and that the *a* axis is parallel to the growth direction of crystals (Figure 4, bottom). The spread angle of the *a* axis is ~30°. We have been unable to map the central plates.

4. Discussion

4.1. Crystal Morphology and Twinning in the Foliated Aragonite. The foliated-aragonite layer is constituted by thin plates with a lath-like shape. They are elongated along the *a* axis and bounded by large basal {001} faces (Figure 2), lateral {010} faces, and less developed front faces, which may be either {110} (arrowhead ending; e.g., *Rokopella*) or {100} (straight ending; e.g., *Micropilina*). The basal planes of the laths are oriented almost parallel (at 2–5°) to the shell surface. Genera differ in crystal morphology. More specifically, if we look at the internal shell areas, the crystals in *Rokopella* are distributed into plates that display better developed faces and are larger (Figure 2g–i) than in the case of *Micropilina* (Figure 2a–f), in which crystals arrange in an intertwined texture (Figure 2d–f). Individual crystals of *Micropilina* show pointed endings with nondeveloped {110} and poorly developed {010} crystals faces. These differences in morphological features give information about the mechanisms and physico-chemical conditions under which crystal growth occurs in these two specimens studied.¹⁰ Those crystal growth features may be explained by assuming that growth occurs at faster rates (higher supersaturation conditions) in *Micropilina* than in the case of the more euhedral crystals of *Rokopella*.

Textural analysis by EBSD shows that foliated aragonite is a highly ordered material. In particular, in *Micropilina*, despite the complex relationships observed, there is a discrete number of constant angular relationships between the orientations of aragonite crystals (Figure 3), which can be explained by twin laws and different epitaxial relations, which are described in detail below. The most frequent association is that of three individual crystals joined by {110} planes forming a cyclic twinning (Figure 2e,f). This type of twinning, here called type I, is characteristic of aragonite and is favored by the pseudo-hexagonal symmetry of aragonite structure (Figure 5a). This twin law explains the occurrence of angular relations close to 120° between the *a* axes of aragonite crystals. However, in many cases, only two of the three crystals are observed (Figure 2f) because the

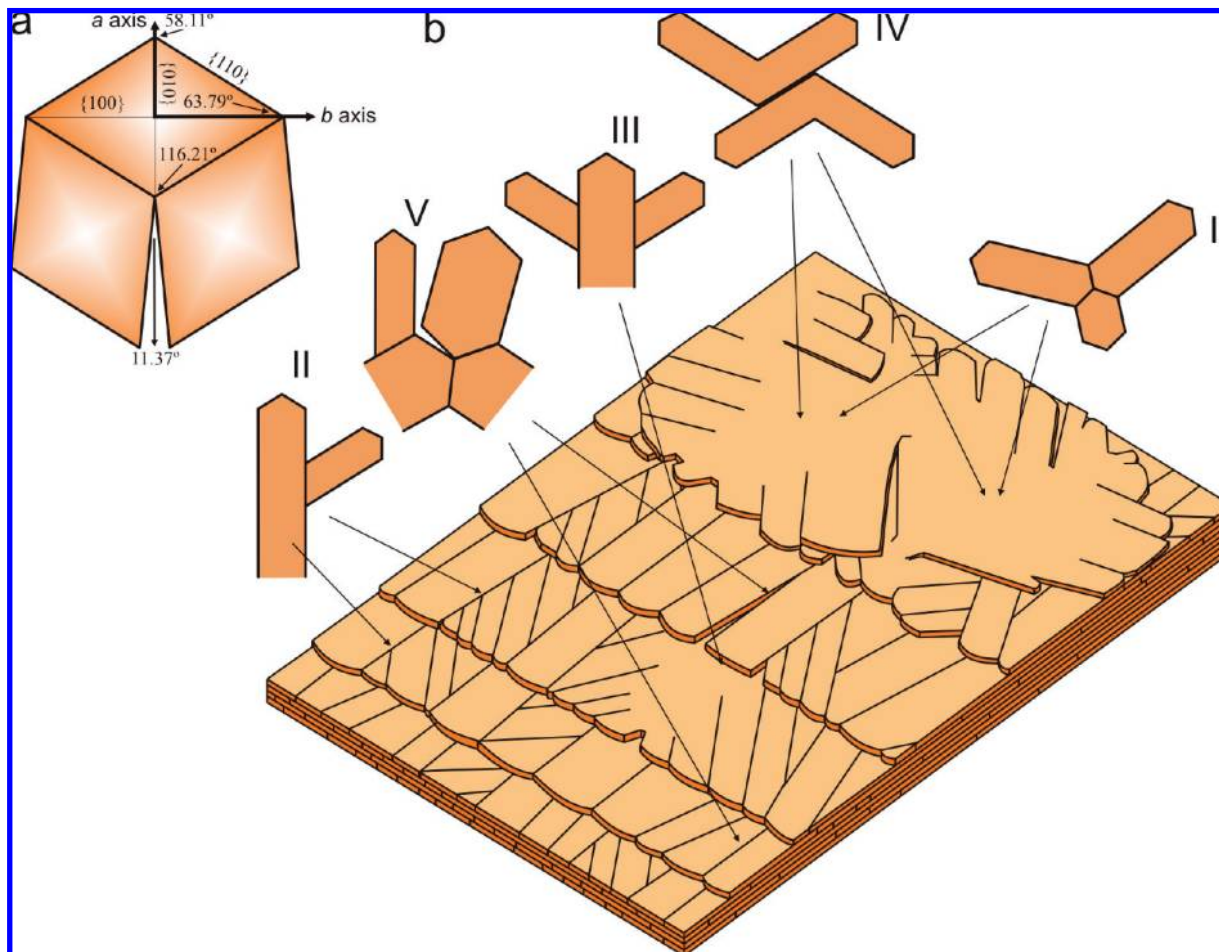


Figure 5. (a) Angular and facial relationships in the typical polycyclic twin of aragonite. (b) Sketch depicting the five angular relationships (types I to V) observed in the foliated aragonite of *Micropilina* and their distribution within the shell.

twinned crystals emerge from the lower lamella, which prevents the backward growth toward the substrate of the third branch (Figures 2f and 5b). Besides this common twinning relationship, other types of relations between aragonite crystals (which usually involve the operation of this main twin law) are also frequently observed in *Micropilina*, and are here described as types II, III, IV, and V (see Figure 5b). These latter ones consist of homoepitaxial intergrowths of aragonite crystals growing on specific crystallographic planes of other aragonite crystals. They are here defined by indicating which crystallographic directions are parallel in both crystals and which is their common interface. Type II relation (e.g., Figure 2b–e) is expressed by $\{110\}_1 \parallel \{010\}_2$ and $\langle 001 \rangle_1 \parallel \langle 001 \rangle_2$, where subscripts refer to aragonite crystals 1 and 2 and the symbol \parallel indicates which crystallographic planes or directions are parallel. Types III (e.g., Figure 2e) and IV (e.g., Figure 2f) twins are represented by $\{001\}_1 \parallel \{001\}_2 \cdot \langle 100 \rangle_1 \parallel \langle 110 \rangle_2$ and $\{010\}_1 \parallel \{010\}_2 \cdot \langle 001 \rangle_1 \parallel \langle 001 \rangle_2$, respectively (Figure 5). Types I to IV produce angular relations in the 100 pole figures at about 60° (Figure 3). However, the 120° angle relationship between aragonite blades typical of types I and IV are visible only in SEM images when we take into consideration the direction to which the crystal arrow-endings are pointing (Figure 2e,f). A final and very frequent relationship (type V) is that in which the a axes of related crystals form an angle of $\sim 12^\circ$ (Figures 2c,e and 3). This angle is the misfit angle between two of the three crystals related by a type I cyclic twin

(Figure 5a). When one of those is also related to a fourth crystal by a type II twinning (Figure 5b), then the 12° angular relation between crystals results.

4.2. Evolution of Crystal Orientation during Shell Growth.

As described above, the angle relationship between a pair of crystals is defined by different twin laws which have been described previously. However, the predominance of the diverse twin types and the orientation of the whole aggregate changes with the distance from a given position in the foliated layer to the shell edge (Figure 2a). Orientation analyses by SEM-EBSD on *Micropilina* show that the angular scattering of the a axis decreases from the shell interior (Figure 3b) to the shell margin (Figure 3a) with aragonite blades becoming preferentially oriented with their elongation axes parallel to the local direction of shell growth (i.e., perpendicular to the shell edge; thick black arrows in Figure 3). Secondary electron images of the inner areas of the shell (Figures 2d–f and 3) display how crystals grow freely, forming small piles, whereas in the outer areas, lamellae arrange step-like and are formed by well-oriented crystals (Figure 2b). In *Rokopella*, a similar ordering pattern is observed, with large pseudo-hexagonal plates forming piles in the shell interior (Figure 2h), whereas laths align with their elongation axis parallel to a preferential direction in the marginal area (Figures 2g and 4), which is tangent to the shell edge in this case. Toward the shell edge, twin types II and V become more frequent to dominant (Figure 3a). The progressive alignment of aragonite crystals is because the

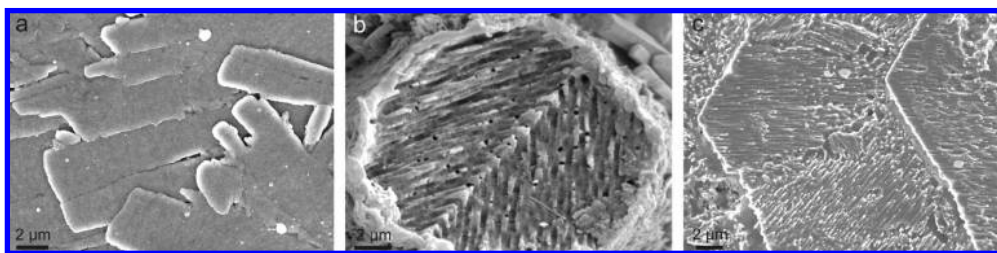


Figure 6. (a). Set of laths with conspicuous growth lines in an internal shell area of *Micropilina arntzi*. (b). Etching lineations along the a axis in an aragonite prism of the bivalve *Lyonsella abyssicola*; it is composed of two twinned crystals with their a axes at $\sim 60^\circ$. (c) Same as in (b) in aragonite plates of the shell interior of the gastropod *Gibbula umbilicalis*; lineations reveal its polycrystalline character and also point to twinning relationships.

growth of crystals is constrained by the step-like arrangement of lamellae, with well-defined growth fronts. Therefore, only those crystals oriented with their a axes nearly perpendicular to the growth front of the lamellae can continue to grow without being intercepted by others.^{5a,11} This results in the disappearance of those twin types with large angular divergence between crystals (types I, III, and IV) toward the edge. The final outcome of this competitive crystal growth process is an aggregate formed by blade-like crystals with their a axes pointing perpendicular to the lamellae growth front and only preserving twin types in which the a axes of related crystals form narrow angles (12° or 60° , at best).

4.3. Structural Controls on the Habit of the Foliated Aragonite. The blade-like morphology of crystals in the foliated aragonite is unique and markedly different from that found in inorganically precipitated aragonite, which usually displays prismatic or fibrous habits, with preferential growth along the c axis.¹² In *Micropilina*, crystals develop along the a axis direction (Figure 2b–f). In *Rokopella*, there are no dendritic features and growth along the a axis is evidenced by EBSD data (Figure 4) as well as by the occurrence of etching lineations (Figure 2i). It is well-known that the habit of crystals is determined by the relative rate of growth along different crystal directions. This implies that the zone directions in the crystal are fast growth directions and that they are usually parallel to structural directions defined by chains of strong bonds.^{13a–d} In the aragonite structure, there are chains of strong bonds along the a axis since the distance between the Ca atoms and the CO_3 groups is the shortest. Therefore, a fast growth along the a axis, as observed in the foliated aragonite of *Rokopella* and, in particular, of *Micropilina*, should be expected, instead of along the c -axis. Does this mean that classical hypotheses on the structural controls of the habit based on the occurrence of the strong bonded interactions in the crystallographic structure explains the crystal growth features observed in *Micropilina* and *Rokopella*?

Growth along the c axis of the aragonite structure must be controlled by the stacking of CO_3 group layers. It is also noteworthy that such groups are separated by only 2.88 Å along the c -axis and that they form groups connected by weak chemical forces (van der Waals forces). The occurrence of such chains could be responsible for the fast growth along the c axis usually observed in aragonite, which must therefore be kinetically favored. Aragonite is the stable polymorph of calcium carbonate at high pressure, which is consistent with the higher coordination for Ca and O in the structure and its greater density compared to calcite (the stable phase under earth-surface conditions). Thus, it is not

surprising that structural explanations of habit based on classical bonded interactions, such as the chemical forces between ions, do not apply to aragonite, and probably nonbonded weak interactions between molecular groups would be more effective in explaining this dense phase.

The structural control on crystal growth also operates in the biological systems, although in many instances the influence on the final habit is secondary. It usually happens that the morphology is controlled by organic molecules which become absorbed onto specific crystallographic faces, with which they have a chemical affinity.¹⁴ In the case of the foliated aragonite of *Micropilina*, the growth is clearly inhibited along both the c and b axes. This is evidenced in individual crystals by the appearance of sharp growth lines on large $\{001\}$ faces, which correspond to the traces of $\{100\}$ faces (Figure 6a). Inhibition is presumably due to the adsorption of organic molecules onto the aragonite $\{001\}$ and $\{010\}$ surfaces. In contrast, the growth along the a axis is not inhibited to any extent. Because the formation of strong bonds along the a axis is energetically favored, there is no affinity for aragonite crystals to incorporate foreign ions or organic molecules along this direction, and thus growth continues undisturbed, resulting in the formation of crystals elongated along this direction. In *Rokopella*, on the other hand, growth along the b axis is not so strictly inhibited as in *Micropilina*, as reflected by the wider plate-like morphology of the crystals of the central area (Figure 2h,i). The ability of the crystals to expand laterally (i.e., along the b axis) (Figures 2g and 4) explains the perfect tiling within each lamella. On the other hand, large spaces between blade-like crystals would occur in the uniaxial array of *Micropilina* crystals near the shell growth front, since lateral expansion of blades is prevented. This explains the abundance of type II twins in this case (Figure 2b), which fill in the available spaces.

Etching lineations along the a axis, here observed in *Rokopella*, are generalized features in biogenic aragonite formed by molluscs, since it has also been observed in nacre¹⁵ and prismatic aragonite (unpublished observations) (Figure 6b,c). They result from differential corrosion and delineate zones that are poorer in organic matter. These features are easily explained because organic molecules become expelled from more mineralized zones along the a axis by the crystallization pressure, being otherwise absorbed within the biogenic crystal along the other, though fast, crystallographic directions.

In conclusion, the foliated aragonite of monoplacophorans shows unique morphological features and crystallographic orientation relationships which are not found in other inorganic or biogenic aragonite-based materials. These unique

features are defined by the structural characteristics of aragonite and by the interaction with specific organic molecules.

Acknowledgment. Serge Gofas (Universidad de Málaga), Anders Warén and Karin Sindemark Kronstedt (Swedish Museum of Natural History) provided specimens. Alicia González-Segura (Universidad de Granada) significantly helped with EBSD analysis. The study was funded by the Research Projects CGL2005-03887, CGL2007-66744-CO2-01 and CGL2007-60549 (MEC) and by the Research Groups RNM 179 and RNM190 (JA).

References

- (1) (a) Taylor, J. D.; Kennedy, W. J.; Hall, A. *Bull. Br. Mus. Nat. Hist. Zool.* **1969**, 3 (Suppl.), 1–125. (b) Carter, J. G. in *Skeletal Biomineralization: Patterns, Processes and Evolutionary Trends*; Carter, J. G., Ed; Van Nostrand Reinhold, New York, 1990; Vol. 1, pp 297–411.
- (2) (a) Weiner, S.; Traub, W. *Phil. Trans. R. Soc. London* **1984**, B304, 421–438. (b) Cartwright, J. H. E.; Checa, A. G. *J. R. Soc. Interface* **2007**, 4, 491–504.
- (3) Addadi, L.; Weiner, S. *Angew. Chem., Int. Ed. Engl.* **1992**, 31, 153–169.
- (4) (a) Belcher, A. M.; Wu, X. H.; Christensen, R. J.; Hansma, P. K.; Stucky, G. D.; Morse, D. E. *Nature* **1996**, 381, 56–58. (b) Falini, G.; Albeck, S.; Weiner, S.; Addadi, L. *Science* **1996**, 271, 67–69. (c) Nudelman, F.; Gotliv, B. A.; Addadi, L.; Weiner, S. *J. Struct. Biol.* **2006**, 153, 176–187.
- (5) (a) Checa, A. G.; Rodríguez-Navarro, A. *Proc. R. Soc. London* **2001**, B268, 771–778. (b) Checa, A. G.; Rodríguez-Navarro, A. *Biomaterials* **2005**, 26, 1071–1079.
- (6) (a) Bevelander, G.; Nakahara, H. *Calcif. Tissue Res.* **1969**, 3, 84–92. (b) Addadi, L.; Joester, D.; Nudelman, F.; Weiner, S. *Chem.—Eur. J.* **2005**, 12, 980–987.
- (7) Peel, J. S. *Bull. Grønlands Geol. Undersøgelse* **1991**, 161, 11–65.
- (8) (a) Schmidt, W. J. in *Scientific Results of the Danish Deep-Sea Expedition round the World 1950–52, Galathea Report*; Bruun, A. F.; Greve, S.; Sparck, R.; Wolff, T., Eds; Danish Science Press: Copenhagen, 1959; Vol. 3, pp 73–76. (b) Erben, H. K.; Flajs, G.; Siehl, A. *Akad. Wiss. Lit., Abh. Math.-Naturwiss. Kl.* **1968**, 1968, 1–24. (c) Meenakshi, V. R.; Hare, P. E.; Watabe, N.; Wilbur, K. M.; Menzies, R. J. *Anton Bruun Rep.* **1970**, 2, 3–12. (d) Urgorri, V.; Garçça-Álvarez, O.; Luque, A. *J. Moll. Stud.* **2005**, 71, 59–66. (e) Warén, A.; Gofas, S. *Zool. Scr.* **1996**, 25, 215–232. (f) Cruz, R.; Weismuller, G.; Farina, M. *Scanning* **2003**, 25, 12–18.
- (9) Checa, A. G.; Ramírez-Rico, J.; González-Segura, A.; Sánchez-Navas, A. *Naturwissenschaften* **2009**, 96, 111–122.
- (10) Sunagawa, I. *Morphology of Crystals*; Terra Scientific Publishing Company: Tokyo, 1987.
- (11) Ubukata, T. *Palaeontology* **1994**, 37, 241–261.
- (12) Reddy, M. M.; Nancollas, G. H. *J. Cryst. Growth* **1976**, 35, 33–38.
- (13) (a) Hartman, P.; Perdok, W. G. *Acta Crystallogr.* **1955**, 8, 49–52. (b) Hartman, P.; Perdok, W. G. *Acta Crystallogr.* **1955**, 8, 521–524. (c) Hartman, P.; Perdok, W. G. *Acta Crystallogr.* **1955**, 8, 525–529. (d) Hartman, P.; Bennema, P. *J. Cryst. Growth* **1980**, 49, 145–156.
- (14) Addadi, L.; Weiner, S. *Proc. Natl. Acad. Sci. U.S.A.* **1985**, 82, 4110–4114.
- (15) Mutvei, H. *Zool. Scr.* **1978**, 7, 287–296.